Rapid Communications

Spin-polarized proton beam generation from gas-jet targets by intense laser pulses

Luling Jin,[1] Meng Wen,[1,*] Xiaomei Zhang,[2,†] Anna Hützen,[3,4] Johannes Thomas,[5] Markus Büscher,[3,4] and Baifei Shen[2,6]

[1]*Department of Physics, Hubei University, Wuhan 430062, China*
[2]*State Key Laboratory of High Field Laser Physics, Shanghai Institute of Optics and Fine Mechanics, Chinese Academy of Sciences, Shanghai 201800, China*
[3]*Peter Grünberg Institut (PGI-6), Forschungszentrum Jülich, Wilhelm-Johnen-Str. 1, 52425 Jülich, Germany*
[4]*Institut für Laser- und Plasmaphysik, Heinrich-Heine-Universität Düsseldorf, Universitätsstr. 1, 40225 Düsseldorf, Germany*
[5]*Institut für Theoretische Physik I, Heinrich-Heine-Universität Düsseldorf, Universitätsstr. 1, 40225 Düsseldorf, Germany*
[6]*Department of Physics, Shanghai Normal University, Shanghai 200234, China*

(Received 30 January 2020; revised 17 June 2020; accepted 27 June 2020; published 23 July 2020)

A method of generating spin-polarized proton beams from a gas jet by using a multipetawatt laser is put forward. With currently available techniques of producing prepolarized monatomic gases from photodissociated hydrogen halide molecules and petawatt lasers, proton beams with energy $\gtrsim$50 MeV and $\approx$80% polarization are proved to be obtained. Two-stage acceleration and spin dynamics of protons are investigated theoretically and by means of fully self-consistent three-dimensional particle-in-cell simulations. Our results predict the dependence of the beam polarization on the intensity of the driving laser pulse. Generation of bright energetic polarized proton beams would open a domain of polarization studies with laser driven accelerators and have potential application to enable effective detection in explorations of quantum chromodynamics.

DOI: 10.1103/PhysRevE.102.011201

The polarization of a beam describes the collective spin state for an ensemble of particles. Since polarized particle beams play important roles in solving a wide variety of scientific and medical problems [1–3], the generation [4] and measurement [5] of polarization observables has a flourishing tradition at conventional particle accelerators. In particular, spin-polarized proton beams enable key measurements in explorations of the quantum-chromodynamics landscape [6,7]. High luminosity is required in such experiments for both high-energy colliders to solve the outstanding proton spin puzzle [8,9] and low-energy colliders to extend Standard Model tests [10]. However, the intensity of the polarized beams is generally limited to several hundred milliamperes [11], which is very difficult to be further increased at a traditional accelerator [4]. Although the beam quality of laser-driven protons are not yet competing with the traditional accelerators, the beam intensity can be increased by several orders of magnitude. Therefore, investigation of spin effects of protons in laser accelerators becomes timely and interesting because it enables new low-cost, compact laser accelerators of polarized proton beams.

With the advent of ultra-intense lasers up to $\approx$10 PW [12–14], plasma accelerators are now capable of providing beams with energies of almost hundred MeV per unit charge [15–21]. There have been multiple theoretical works on how to generate polarized beams in laser-driven accelerators [22–27]. These show that underdense plasmas provide a unique opportunity for generation of polarized beams already at existing laser facilities, thanks to recent experimental progress of producing polarized atomic hydrogen gases with densities above 10^{19} cm^{-3} [28]. Although such prepolarized gases can be used in principle to produce multi-MeV proton beams [29–32], an intuitive and optimized acceleration regime and a comprehensive understanding of the acceleration mechanisms is still pending.

In this rapid communication, we demonstrate a laser-driven polarized proton acceleration by means of full three-dimensional (3D) particle-in-cell (PIC) simulations using a basic scenario with available ultra-intense lasers and prepolarized gases. The schematic diagram (see also Refs. [22,25]) is shown in Fig. 1. The laser system comprises a weak circularly polarized UV laser to generate spin-polarized atoms via photodissociation, and an intense laser to accelerate protons. The accelerated proton beam can be depolarized via asynchronous spin precession in inhomogeneous electromagnetic fields of laser driven plasmas. Using a gaseous HCl target with molecular density $\approx 10^{19}$ cm^{-3} and a 1.3 petawatt (PW) laser as an example, the energy of accelerated polarized protons can be as high as 50 MeV, with a beam polarization above 80%. The corresponding phase-space distribution and the spin spread of accelerated protons are shown in Fig. 2. As will be seen below, the energy increases with the power of the driving laser, while the polarization of the beam is almost preserved.

We have proposed a related conceptual setup in Ref. [22], however, several criteria have to be satisfied for the success of laser-induced spin-polarized beam acceleration. First, the parameters assumed in the simulations can be realized in experiments. Second, protons are accelerated effectively in the setup with a polarized or polarizable target. Third, a high

*wenmeng@hubu.edu.cn
†zhxm@siom.ac.cn

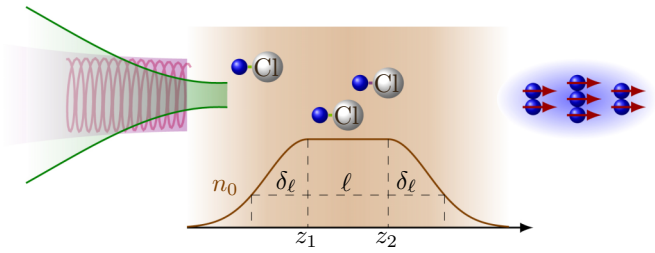

FIG. 1. A schematic diagram showing laser acceleration of polarized protons from a dense hydrogen chloride gas target (brown). Molecules are initially aligned along z axis via a weak optical laser. Blue and white balls represent nuclei of hydrogen and chlorine atoms, respectively. Before the acceleration driven by an intense laser beam (indicated by the green area), a weak circularly polarized UV laser (purple area) is used to generate the polarized atoms along the longitudinal direction via molecular photodissociation. The brown curve indicates the initial density distribution of the gas-jet target. The polarized proton beam is shown on the right (blue) with arrows (red) presenting the polarization direction.

degree of polarization of the accelerated protons is retained. The first criterion is met by adopting currently available PW lasers and a gas jet of polarized atoms with hydrogen density $\approx 10^{19}$ cm^{-3}. The latter can be built via laser photodissociation with circularly polarized UV laser pulses (see Fig. 1) [28]. After the molecules are dissociated to polarized atoms, the polarization is transferred from electrons to nuclei within a few 100 ps and oscillates between electrons and nuclei afterwards. Experiments should be designed such that the polarized gas is fully ionized by the PW laser when the hydrogen nuclei acquire a high degree of polarization. The delay between the UV laser and the driving pulse for ion

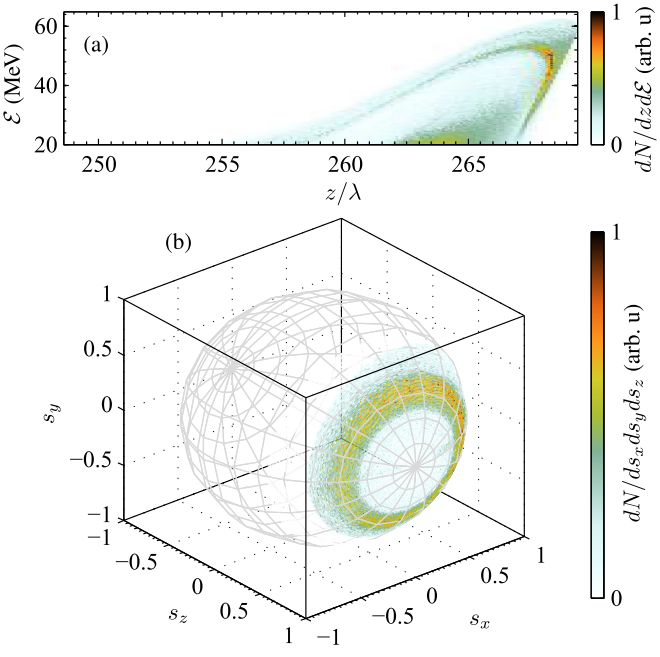

FIG. 2. Snapshots at $t = 330\lambda/c$ of (a) phase-space distribution, and (b) spin spread of protons with energy $\mathcal{E} \geqslant 20$ MeV on the Bloch sphere. Simulation parameters can be found in the text.

acceleration should therefore be carefully controlled, which is accessible by splitting one laser beam [25] or by combining different laser systems [22]. The remaining two criteria of efficient proton acceleration and small spin smearing under current available experiment conditions will be demonstrated below with 3D-PIC simulations.

Acceleration and spin precession of protons are investigated by employing the EPOCH code [33] which has been extended by spin effects [34–36]. The spin state of a charged particle with kinetic momentum $\boldsymbol{p}$ and velocity $\boldsymbol{v}$ is characterized classically by the unit vector $\boldsymbol{s} = (c_1^* c_2 + c_1 c_2^*, ic_1 c_2^* - ic_1^* c_2, |c_1|^2 - |c_2|^2)$, with $c_1|\uparrow> + c_2|\downarrow>$ denoting the arbitrary spin state on the Bloch sphere of Fig. 2(b) and $|\uparrow>$ a spin direction parallel to the z axis. Furthermore, the Landau-Lifshitz equation $d\boldsymbol{p}/dt = \boldsymbol{F}_L + \boldsymbol{F}_R$ is applied to calculate the motion of electrons in the radiation-dominated regime driven by PW lasers [37]. Here $\boldsymbol{F}_L = -q(\boldsymbol{E} + \boldsymbol{v} \times \boldsymbol{B})$ is the Lorentz force and $\boldsymbol{F}_R \approx q^4/(6\pi\varepsilon_0 m^2 c^5)[(\boldsymbol{v} \cdot \boldsymbol{E}/c)^2 - (\boldsymbol{E} + \boldsymbol{v} \times \boldsymbol{B})^2]\gamma^2 \boldsymbol{v}$ is the Landau-Lifshitz force, with γ being the relativistic Lorentz factor, c the speed of light in vacuum, and m and q the electron mass and charge, respectively.

The 3D-PIC simulations are performed with a moving box of size $100\lambda \times 80\lambda \times 80\lambda$ represented by a $1000 \times 400 \times 400$ grid at the speed of light c and a total pseudoparticle number of 8×10^8. The laser pulse for proton acceleration (green area in Fig. 1) with a bi-Gaussian envelope $\boldsymbol{a} = \boldsymbol{e}_x a_0 \exp[-(t - z/c + z_0/c)^2/\tau_0^2 - r^2/w_0^2]$ and a focal position z_0 propagates along the z axis, where the laser amplitude $a_0 = 25$, focal radius $w_0 = 10\lambda$, wavelength $\lambda = 800$ nm, and temporal duration $\tau_0 = 10\lambda/c$. To reach a high acceleration efficiency, the laser pulse is focused to the left boundary of the gas target $z_0 = z_1 = 50\lambda$. The target is assumed to be a fully ionized plasma of HCl gas, with all protons initially polarized along the z axis $\eta_0 = \langle \boldsymbol{s}_0 \rangle \cdot \boldsymbol{e}_z = 1$. Its density profile, as shown by the brown curve in Fig. 1, is a uniform plateau with steep edges [32,38–40]. The length of the target is $\ell = z_2 - z_1 = 200\lambda$. The density gradient at the edge is expressed as $n = n_0 \exp[-(z - z_i)^2/\delta_\ell^2]$ with $\delta_\ell = 5\lambda$, where $i = 1$ and 2 correspond to the left and right boundaries of the target, respectively. In the following simulations, gas jets with electron density $n_0 = 0.36 n_c$ are applied where $n_c = \varepsilon_0 m\omega^2/e^2$ is the critical plasma density, ε_0 is the vacuum permittivity, and $\omega = 2\pi c/\lambda$ is the laser frequency. One should note that the proton density n_p is lower than the plasma density, i.e., $n_p = n_0/(Z_H + Z_{Cl}) \approx 3.48 \times 10^{19}$ cm^{-3}, with charge numbers of hydrogen $Z_H = 1$ and chlorine $Z_{Cl} = 17$.

Acceleration of protons and spin precession takes place within the plasma channel driven by the intense laser. A plasma channel is formed by ponderomotive expulsion of charge lying within the laser's path, as a relativistic self-focusing effect in high-power laser-plasma interactions when the laser power exceeds the critical value $P_c = 17 n_c/n_0$ GW. When a laser pulse with even higher power propagates in an underdense plasma, $P_L = 21.49 a_0^2 w_0^2/\lambda^2$ GW $\gg P_c$, an additional central electron filament is enclosed in the evacuated channel [41,42]. The displacement of electrons introduces a radial electric field E_r in the plasma channel, as well as an azimuthal magnetic field around the channel axis B_ϕ. The magnetic field B_ϕ is represented in Fig. 3(a) by B_x in the z-y plane. Effected by the space-charge field E_r, ions also

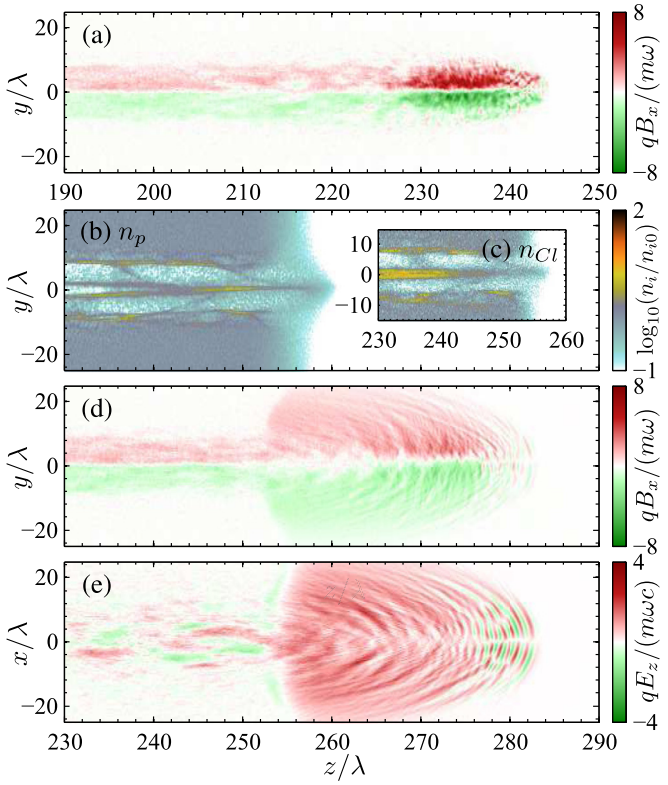

FIG. 3. Snapshots of (a) azimuthal magnetic field at $t = 250\lambda/c$, (b) proton density, (c) chlorine nuclei density, (d) azimuthal magnetic field, and (e) longitudinal electric field at $t = 290\lambda/c$.

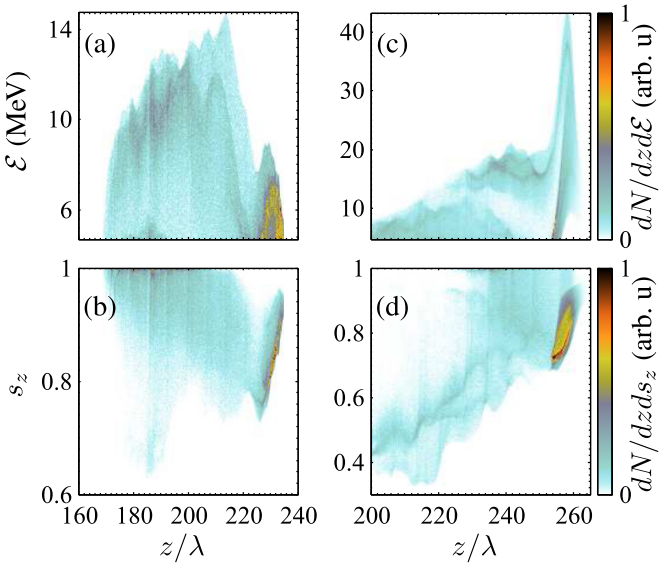

FIG. 4. Density plot of energetic protons (with $\mathcal{E} \geqslant 5$ MeV) in (a), (c) phase space and (b), (d) space with spin component s_z and z axis. Panels (a), (b) and (c), (d) correspond to density plots at $t = 250\lambda/c$ and $t = 290\lambda/c$, respectively.

move into the filament along the channel axis [43]. Due to the small charge-to-mass ratio of ions, they converge towards the center on a longer timescale as compared with the electrons. More specifically, the electron filament appears inside the laser fields, while the proton filament forms behind the laser pulse but in front of the chlorine nuclei filament. Figures 3(b) and 3(c) show that the proton filament is found around $240 \lesssim x/\lambda \lesssim 260$, and the filament of chlorine nuclei lies around $x \lesssim 240\lambda$. Because of the different responses of particles, longitudinal and radial space-charge fields are formed within the plasma channel. As a results, the protons are accelerated in forward and transverse directions under the actions of the electrons in front and the chlorine nuclei behind. The advantage of the admixture of chlorine is analogous to the case investigated in Ref. [29].

In addition to the first-stage acceleration in the plasma channel, we find a second effect at the rear end of the gas jet, which enhances the proton energies even more significantly. When the electrons driven by the laser pulse pass though the rear boundary, the azimuthal magnetic field expands into the vacuum under large angles. Transverse expansion of the magnetic field generates a strong longitudinal field according to Faraday's law, as shown in Figs. 3(d) and 3(e). The focused protons in the filament near the rear boundary are then accelerated strongly. This secondary acceleration is known as magnetic vortex acceleration [44–46].

Figures 4(a) and 4(b) present effects of the proton acceleration in the plasma channel (with $z < z_2$), and the spin distribution of energetic protons, respectively. It indicates at $t = 250\lambda/c$ many energetic protons start to converge to the front of the proton filament around $z_f = 230\lambda$. The energy of these *front protons* is less than 10 MeV. In contrast to that, the *tail protons* which converge to the filament before ($t < 250\lambda/c$) are accelerated further to energies beyond 10 MeV but sit far behind the driven laser with $z < z_f$. The spin precession for these front protons and tail protons play different roles, as will be discussed below. The PIC simulations have provided clear evidence for the strong magnetic field in the laser-driven plasma channel, as shown in Figs. 3(a) and 3(c). Due to the cylindrical symmetry of the azimuthal magnetic field in the plasma channel, the transverse spin components, s_x and s_y, spread symmetrically. This concurs with the spin distribution on the Bloch sphere shown in Fig. 2(b). The polarization of the collected proton sample is thus determined by the longitudinal spin component $P = \langle s_z \rangle$. Note that depolarization via direct precession of protons is dominant in laser accelerators and the depolarization rate of protons in plasmas via binary collisions $\approx 10^{-22} n_{\mathrm{cm3}} \sqrt{T_{\mathrm{eV}}}\ \mathrm{s}^{-1}$ is negligibly small because of the applied low densities and low temperatures [47], where T_{eV} is the temperature in units of electronvolts and n_{cm3} is the plasma density in units of cm^{-3}.

Spin precession is calculated in the PIC simulations with the Thomas-Bargmann-Michel-Telegdi equation [48,49]

$$\frac{d\boldsymbol{s}}{dt} = \frac{q}{M}\boldsymbol{s} \times \left[\left(G + \frac{1}{\gamma} \right) \boldsymbol{B} - \frac{G\gamma \boldsymbol{v} \cdot \boldsymbol{B}}{\gamma + 1} \frac{\boldsymbol{v}}{c^2} - \left(G + \frac{1}{\gamma + 1} \right) \frac{\boldsymbol{v}}{c^2} \times \boldsymbol{E} \right], \tag{1}$$

where $G \approx 1.79$ is the anomalous magnetic moment of the proton and M and is the proton mass. Simulations as shown in Figs. 4(a) and 4(c) indicate $\gamma - 1 \approx 10^{-2}$ and $|\boldsymbol{v}|/c \approx 10^{-1}$ for accelerated protons. The spin of protons in the filament can be roughly estimated via $s_z \approx 1 - \int_0^{\tau} dt (q/M)(G+1) B_\phi$,

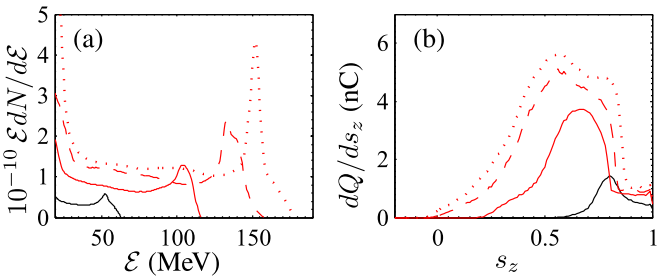

FIG. 5. Snapshots at $t = 330\lambda/c$ of (a) Energy spectra and (b) spin distribution of accelerated protons with $\mathcal{E} \geqslant 20$ MeV in cases with $a_0 = 25$, 50, 75, and 100, which are presented with solid-black, solid-red, dashed-red, and dotted-red curves, respectively.

with τ being the time duration for proton to move to the axis under the radial electric field E_r. It explains a significant spin precession in the simulations. First, due to the small proton velocity, the precession time τ in the magnetic fields is long; second, the anomalous magnetic moment G is larger than that of electrons; third, spin precession of a proton is directly affected by its trajectory and the field structure, where the dominant azimuthal magnetic field $B_\phi \sim 8m\omega/q$ in the plasma channel is strong.

When the protons are focused to the axis, the longitudinal spin component of front protons around $z = z_f$ decreases to $s_z \sim 80\%$ as shown in Fig. 4(b). This indicates that the magnetic field is strong enough to significantly depolarize the accelerated beam protons. In the channel driven by lasers with $a_0 = 25$, about 80 % of the polarization is retained. For tail protons with further acceleration in the channel $z < z_f$ in Fig. 4(a), they conserve their momentum and continue to travel radially away after they cross the laser axis, which results in a change of the direction of B_ϕ. Figure 4(b) shows larger s_z of these protons, indicating that they precess back to their initial direction along z.

At the rear boundary of the gas jet, protons experience the second-stage acceleration. When the front of the proton filament passes z_2 immediately after the electrons and enters the region with strong longitudinal electric field [see Figs. 3(c) and 3(d)], corresponding protons are accelerated intensely to 40 MeV [see Fig. 4(c)]. Meanwhile, the spin vector of front protons precesses roughly at the same rate (≈80%) compared with the front protons in the plasma channel, see Figs. 4(b) and 4(d). Differently, the more energetic tail protons in the channel leave too far behind the electrons. When they pass z_2, the magnetic-vortex-induced electric field becomes too weak to accelerate protons for its limited lifetime. Figure 2(a) indicates that only the front protons in the filament are accelerated to an energy >20 MeV. In other words, the tail protons neither contribute to the final accelerated proton beam nor to the beam polarization.

After the second-stage acceleration at the rear boundary of the gas jet, electromagnetic fields around the accelerated beam quickly decay. The magnetic field as well as the electric field around the propagating axis become too weak to affect the protons after $t = 330\lambda/c$. Thus both energy and polarization of the proton beam remains constant. Properties of the final accelerated proton beams with $\mathcal{E} \geqslant 20$ MeV are presented in Fig. 2 and solid-black lines in Fig. 5. Applying laser systems with a power of 1.3 PW, the protons are accelerated to tens of MeV with a peak at 53 MeV, while polarization of $P = 82\,\%$ is retained. The corresponding proton current shown in Fig. 2(a) is of the order of 10 kA. Simulations with lower target density ($n_p \approx 10^{18}$ cm^{-3}) results in lower charge of the accelerated polarized proton beam (not shown). The accelerated energy and beam charge, as listed in Table I, increase with the driving laser intensity. As a polarized proton source, one may not boost the proton energy by enhancing the plasma density as with other magnetic-vortex accelerations [44]. Therefore, the beam energy does not increase linearly with the laser power. Figure 5(b) implies that this nonlinear dependence on the laser power also applies to the proton depolarization. Low-intensity laser pulses or the rising edges of the main pulse with much lower power in a real experiment are not intense enough to accelerate and depolarize the proton beams from a gas jet. While totally polarized HCl gases are possibly produced experimentally [50,51], the beam polarization can be reduced to $\eta_0 P$ when $\eta_0 < 1$. A systematic study of other experimental parameters, like the inhomogeneity of initial polarization $\eta_0(x, y, z)$, pulse intensity and duration, or target density and length, on the proton energy distribution, flux, and polarization is under way and will be the subject of a forthcoming presentation. More importantly, as shown in Fig. 5(b) and Table I, more than 50% of the proton beam polarization driven by PW lasers can be sustained. Although the beam quality needs to be further improved, effective detection in high-energy experiments may benefit from the high luminosity of the laser-driven proton beams.

TABLE I. Polarized beams accelerated by PW lasers. Results from Fig. 5 are compared and the parameters used are given. Here, P_L is the laser power, $\mathcal{E}_p$ is the peak proton energy, Q is the total charge, P is the beam polarization.

a_0	P_L [PW]	$\mathcal{E}_p$ [MeV]	Q [nC]	P [%]
25	1.34	53	0.26	82
50	5.37	105	1.3	65
75	12.1	133	2.4	57
100	21.5	152	3.1	56

We would like to thank Z. Y. Li for helpful discussions. This work was supported by the Ministry of Science and Technology of the People's Republic of China (Grants No. 2018YFA0404803 and No. 2016YFA0401102), the National Natural Science Foundation of China (Grants No. 11674339, No. 11922515, and No. 11935008), the Strategic Priority Research Program of the Chinese Academy of Sciences (Grant No. XDB16), and the Innovation Program of Shanghai Municipal Education Commission. The work of M.B. and A.H. has been carried out in the framework of the *Ju*SPARC (Jülich Short-Pulse Particle and Radiation Center) and has been supported by the ATHENA (Accelerator Technology Helmholtz Infrastructure) consortium.

[1] T. R. Gentile, P. J. Nacher, B. Saam, and T. G. Walker, Optically polarized ^{3}He, Rev. Mod. Phys. **89**, 045004 (2017).

[2] M. S. Safronova, D. Budker, D. DeMille, Derek F. Jackson Kimball, A. Derevianko, and C. W. Clark, Search for new physics with atoms and molecules, Rev. Mod. Phys. **90**, 025008 (2018).

[3] G. Moortgat-Pick *et al.*, The role of polarized positrons and electrons in revealing fundamental interactions at the linear collider, Phys. Rep. **460**, 131 (2008).

[4] S. R. Mane, Y. M. Shatunov, and K. Yokoya, Spin-polarized charged particle beams in high-energy accelerators, Rep. Prog. Phys. **68**, 1997 (2005).

[5] P. Adlarson, W. Augustyniak, W. Bardan, M. Bashkanov, F. S. Bergmann, M. Berłowski, H. Bhatt, M. Büscher, H. Calén, I. Ciepał *et al.* (WASA-at-COSY Collaboration and SAID Data Analysis Center), Evidence for a New Resonance from Polarized Neutron-Proton Scattering, Phys. Rev. Lett. **112**, 202301 (2014).

[6] L. Adamczyk, J. K. Adkins, G. Agakishiev, M. M. Aggarwal, Z. Ahammed, I. Alekseev, A. Aparin, D. Arkhipkin, E. C. Aschenauer, A. Attri *et al.* (STAR Collaboration), Measurement of the Transverse Single-Spin Asymmetry in $p^\uparrow + p \to W^\pm/Z^0$ at RHIC, Phys. Rev. Lett. **116**, 132301 (2016).

[7] E. C. Aschenauer, S. Fazio, J. H. Lee, H. Mäntysaari, B. S. Page, B. Schenke, T. Ullrich, R. Venugopalan, and P. Zurita, The electron-ion collider: Assessing the energy dependence of key measurements, Rep. Prog. Phys. **82**, 024301 (2019).

[8] D. de Florian, R. Sassot, M. Stratmann, and W. Vogelsang, Evidence for Polarization of Gluons in the Proton, Phys. Rev. Lett. **113**, 012001 (2014).

[9] C. Alexandrou, M. Constantinou, K. Hadjiyiannakou, K. Jansen, C. Kallidonis, G. Koutsou, A. V. Avilés-Casco, and C. Wiese, Nucleon Spin and Momentum Decomposition using Lattice QCD Simulations, Phys. Rev. Lett. **119**, 142002 (2017).

[10] D. Androic *et al.* (The Jefferson Lab Qweak Collaboration), Precision measurement of the weak charge of the proton, Nature (London) **557**, 207 (2018).

[11] A. Accardi, J. L. Albacete, M. Anselmino, N. Armesto, E. C. Aschenauer, A. Bacchetta, D. Boer, W. K. Brooks, T. Burton, N. B. Chang *et al.*, Electron-ion collider: The next QCD frontier, Eur. Phys. J. A **52**, 268 (2016).

[12] V. Yanovsky, V. Chvykov, G. Kalinchenko, P. Rousseau, T. Planchon, T. Matsuoka, A. Maksimchuk, J. Nees, G. Cheriaux, G. Mourou *et al.*, Ultra-high intensity 300-TW laser at 0.1 Hz repetition rate, Opt. Express **16**, 2109 (2008).

[13] Z. Guo, L. Yu, J. Wang, C. Wang, Y. Liu, Z. Gan, W. Li, Y. Leng, X. Liang, and R. Li, Improvement of the focusing ability by double deformable mirrors for 10-PW-level Ti:sapphire chirped pulse amplification laser system, Opt. Express **26**, 26776 (2018).

[14] J. W. Yoon, C. Jeon, J. Shin, S. K. Lee, H. W. Lee, I. W. Choi, H. T. Kim, J. H. Sung, and C. H. Nam, Achieving the laser intensity of $5.5 \times 10^{22}\mathrm{W/cm}^2$ with a wavefront-corrected multi-PW laser, Opt. Express **27**, 20412 (2019).

[15] F. Wagner, O. Deppert, C. Brabetz, P. Fiala, A. Kleinschmidt, P. Poth, V. A. Schanz, A. Tebartz, B. Zielbauer, M. Roth *et al.*, Maximum Proton Energy above 85 MeV from the Relativistic Interaction of Laser Pulses with Micrometer thick CH_2 targets, Phys. Rev. Lett. **116**, 205002 (2016).

[16] I. J. Kim, K. H. Pae, I. W. Choi, C.-L. Lee, H. T. Kim, H. Singhal, J. H. Sung, S. K. Lee, H. W. Lee, P. V. Nickles *et al.*, Radiation pressure acceleration of protons to 93 MeV with circularly polarized petawatt laser pulses, Phys. Plasmas **23**, 070701 (2016).

[17] H. Zhang, B. F. Shen, W. P. Wang, S. H. Zhai, S. S. Li, X. M. Lu, J. F. Li, R. J. Xu, X. L. Wang, X. Y. Liang *et al.*, Collisionless Shock Acceleration of High-Flux Quasimonoenergetic Proton Beams Driven by Circularly Polarized Laser Pulses, Phys. Rev. Lett. **119**, 164801 (2017).

[18] P. Hilz, T. M. Ostermayr, A. Huebl, V. Bagnoud, B. Borm, M. Bussmann, M. Gallei, J. Gebhard, D. Haffa, J. Hartmann *et al.*, Isolated proton bunch acceleration by a petawatt laser pulse, Nat. Commun. **9**, 423 (2018).

[19] A. Higginson, R. J. Gray, M. King, R. J. Dance, S. D. R. Williamson, N. M. H. Butler, R. Wilson, R. Capdessus, C. Armstrong, J. S. Green *et al.*, Near-100 MeV protons via a laser-driven transparency-enhanced hybrid acceleration scheme, Nat. Commun. **9**, 724 (2018).

[20] W. J. Ma, I. J. Kim, J. Q. Yu, I. W. Choi, P. K. Singh, H. W. Lee, J. H. Sung, S. K. Lee, C. Lin, Q. Liao *et al.*, Laser Acceleration of Highly Energetic Carbon Ions using a Double-Layer Target Composed of Slightly Underdense Plasma and Ultrathin Foil, Phys. Rev. Lett. **122**, 014803 (2019).

[21] S. D. Kraft, L. Obst, J. Metzkes-Ng, H.-P. Schlenvoigt, K. Zeil, S. Michaux, D. Chatain, J.-P. Perin, S. N. Chen, J. Fuchs, M. Gauthier, T. E. Cowan, and U. Schramm, First demonstration of multi-MeV proton acceleration from a cryogenic hydrogen ribbon target, Plasma Phys. Control. Fusion **60**, 044010 (2018).

[22] A. Hützen, J. Thomas, J. Böker, R. Engels, R. Gebel, A. Lehrach, A. Pukhov, T. P. Rakitzis, D. Sofikitis, M. Büscher *et al.*, Polarized proton beams from laser-induced plasmas, High Power Laser Sci. Eng. **7**, e16 (2019).

[23] M. Büscher, A. Hützen, I. Engin, J. Thomas, A. Pukhov, J. Böker, R. Gebel, A. Lehrach, R. Engels, T. Peter Rakitzis, and D. Sofikitis, Polarized proton beams from a laser-plasma accelerator, Int. J. Mod. Phys. A **34**, 1942028 (2019).

[24] Y.-F. Li, R. Shaisultanov, K. Z. Hatsagortsyan, F. Wan, C. H. Keitel, and J.-X. Li, UltraRelativistic Electron-Beam Polarization in Single-Shot Interaction with an Ultraintense Laser Pulse, Phys. Rev. Lett. **122**, 154801 (2019).

[25] M. Wen, M. Tamburini, and C. H. Keitel, Polarized Laser-Wakefield-Accelerated Kiloampere Electron Beams, Phys. Rev. Lett. **122**, 214801 (2019).

[26] Y. Wu, L. Ji, X. Geng, Q. Yu, N. Wang, B. Feng, Z. Guo, W. Wang, C. Qin, X. Yan, L. Zhang, J. Thomas, A. Hützen, A. Pukhov, M. Büscher, B. Shen, and R. Li, Polarized electron acceleration in beam-driven plasma wakefield based on density down-ramp injection, Phys. Rev. E **100**, 043202 (2019).

[27] J. Thomas, A. Hützen, A. Lehrach, A. Pukhov, L. Ji, Y. Wu, X. Geng, and M. Büscher, Scaling laws for the depolarization time of relativistic particle beams in strong fields, Phys. Rev. Accel. Beams **23**, 064401 (2020).

[28] D. Sofikitis, C. S. Kannis, G. K. Boulogiannis, and T. P. Rakitzis, Ultrahigh-Density Spin-Polarized H and D Observed via Magnetization Quantum Beats, Phys. Rev. Lett. **121**, 083001 (2018).

[29] B. Shen, Y. Li, M. Y. Yu, and J. Cary, Bubble regime for ion acceleration in a laser-driven plasma, Phys. Rev. E **76**, 055402(R) (2007).

[30] X. Zhang, B. Shen, L. Zhang, J. Xu, X. Wang, W. Wang, L. Yi, and Y. Shi, Proton acceleration in underdense plasma by ultraintense Laguerre–Gaussian laser pulse, New J. Phys. **16**, 123051 (2014).

[31] Y. Wan, I. A. Andriyash, J. F. Hua, C.-H. Pai, W. Lu, W. B. Mori, C. Joshi, and V. Malka, Two-stage laser acceleration of high quality protons using a tailored density plasma, Phys. Rev. Accel. Beams **22**, 021301 (2019).

[32] I. Engin, Z. M. Chitgar, O. Deppert, L. D. Lucchio, R. Engels, P. Fedorets, S. Frydrych, P. Gibbon, A. Kleinschmidt, A. Lehrach, R. Maier, D. Prasuhn, M. Roth, F. Schlüter, C. M. Schneider, T. Stöhlker, K. Strathmann, and M. Büscher, Laser-induced acceleration of helium ions from unpolarized gas jets, Plasma Phys. Control. Fusion **61**, 115012 (2019).

[33] T. D. Arber, K. Bennett, C. S. Brady, A. Lawrence-Douglas, M. G. Ramsay, N. J. Sircombe, P. Gillies, R. G. Evans, H. Schmitz, A. R. Bell *et al.*, Contemporary particle-in-cell approach to laser-plasma modelling, Plasma Phys. Control. Fusion **57**, 113001 (2015).

[34] J. Zamanian, M. Stefan, M. Marklund, and G. Brodin, From extended phase space dynamics to fluid theory, Phys. Plasmas **17**, 102109 (2010).

[35] M. Wen, H. Bauke, and C. H. Keitel, Identifying the Stern-Gerlach force of classical electron dynamics, Sci. Rep. **6**, 31624 (2016).

[36] M. Wen, C. H. Keitel, and H. Bauke, Spin-one-half particles in strong electromagnetic fields: Spin effects and radiation reaction, Phys. Rev. A **95**, 042102 (2017).

[37] L. D. Landau and E. M. Lifshitz, *The Classical Theory of Fields* (Butterworth-Heinemann, Oxford, 1980).

[38] S. Semushin and V. Malka, High density gas jet nozzle design for laser target production, Rev. Sci. Instrum. **72**, 2961 (2001).

[39] K. Schmid and L. Veisz, Supersonic gas jets for laser-plasma experiments, Rev. Sci. Instrum. **83**, 053304 (2012).

[40] S. Lorenz, G. Grittani, E. Chacon-Golcher, C. M. Lazzarini, J. Limpouch, F. Nawaz, M. Nevrkla, L. Vilanova, and T. Levato, Characterization of supersonic and subsonic gas targets for laser wakefield electron acceleration experiments, Matter Radiat. Extrem. **4**, 015401 (2019).

[41] K. I. Popov, W. Rozmus, V. Y. Bychenkov, N. Naseri, C. E. Capjack, and A. V. Brantov, Ion Response to Relativistic Electron Bunches in the Blowout Regime of Laser-Plasma Accelerators, Phys. Rev. Lett. **105**, 195002 (2010).

[42] L. L. Ji, A. Pukhov, I. Y. Kostyukov, B. F. Shen, and K. Akli, Radiation-Reaction Trapping of Electrons in Extreme Laser Fields, Phys. Rev. Lett. **112**, 145003 (2014).

[43] F. Sylla, A. Flacco, S. Kahaly, M. Veltcheva, A. Lifschitz, G. Sanchez-Arriaga, E. Lefebvre, and V. Malka, Anticorrelation between Ion Acceleration and Nonlinear Coherent Structures from Laser-Underdense Plasma Interaction, Phys. Rev. Lett. **108**, 115003 (2012).

[44] T. Nakamura, S. V. Bulanov, T. Z. Esirkepov, and M. Kando, High-Energy Ions from Near-Critical Density Plasmas via Magnetic Vortex Acceleration, Phys. Rev. Lett. **105**, 135002 (2010).

[45] S. Kawata, T. Nagashima, M. Takano, T. Izumiyama, D. Kamiyama, D. Barada, Q. Kong, Y. J. Gu, P. X. Wang, Y. Y. Ma *et al.*, Controllability of intense-laser ion acceleration, High Power Laser Sci. Eng. **2**, e4 (2014).

[46] J. Park, S. S. Bulanov, J. Bin, Q. Ji, S. Steinke, J.-L. Vay, C. G. R. Geddes, C. B. Schroeder, W. P. Leemans, T. Schenkel, and E. Esarey, Ion acceleration in laser generated megatesla magnetic vortex, Phys. Plasmas **26**, 103108 (2019).

[47] R. Kulsrud, E. Valeo, and S. Cowley, Physics of spin-polarized plasmas, Nucl. Fusion **26**, 1443 (1986).

[48] L. H. Thomas, The motion of the spinning electron, Nature (London) **117**, 514 (1926).

[49] V. Bargmann, V. L. Telegdi, and L. Michel, Precession of the Polarization of Particles Moving in a Homogeneous Electromagnetic Field, Phys. Rev. Lett. **2**, 435 (1959).

[50] T. P. Rakitzis, P. C. Samartzis, R. L. Toomes, T. N. Kitsopoulos, A. Brown, G. G. Balint-Kurti, O. S. Vasyutinskii, and J. A. Beswick, Spin-polarized hydrogen atoms from molecular photodissociation, Science **300**, 1936 (2003).

[51] D. Sofikitis, P. Glodic, G. Koumarianou, H. Jiang, L. Bougas, P. C. Samartzis, A. Andreev, and T. P. Rakitzis, Highly Nuclear-Spin-Polarized Deuterium Atoms from the UV Photodissociation of Deuterium Iodide, Phys. Rev. Lett. **118**, 233401 (2017).